Electrochemistry Communications 36 (2013) 29–32

Contents lists available at ScienceDirect

Electrochemistry Communications

journal homepage: www.elsevier.com/locate/elecom

Short communication

Improved rate capability of Si–C composite anodes by boron doping for lithium-ion batteries

Ran Yi, Jiantao Zai, Fang Dai, Mikhail L. Gordin, Donghai Wang *

Department of Mechanical and Nuclear Engineering, The Pennsylvania State University, University Park, PA 16802, USA

ARTICLE INFO

Article history:
Received 17 July 2013
Received in revised form 15 August 2013
Accepted 4 September 2013
Available online 12 September 2013

Keywords:
Boron doping
Si–C composite
Rate capability
Anode
Lithium-ion battery

ABSTRACT

We report a novel strategy to enhance the rate capability of Si–C composite by facile boron doping. Boron doping was confirmed by X-ray powder diffraction (XRD), X-ray photoelectron spectroscopy (XPS) and Raman spectroscopy. The boron-doped Si–C composite shows much improved rate capability, delivering a capacity of 575 mAh/g at 6.4 A/g without any external carbon additive, 80% higher than that of undoped composite. Electrochemical impedance spectroscopy (EIS) measurement shows that boron-doped Si–C composite has lower charge transfer resistance, which helps improve its rate capability.

1. Introduction

The fast-growing demands of portable electronics and electric vehicles require lithium-ion batteries (LIBs) with high energy and power densities [1]. The low specific capacity (372 mAh/g) of graphite, a common anode material in commercial LIBs, is a major barrier to meeting these demands [2]. Silicon has been investigated as one of the most promising alternatives to graphite due to its high specific capacity (>3500 mAh/g) and abundance [3]. However, silicon suffers from low power output, mainly because its electronic conductivity is low [4].

Great efforts have been devoted to enhancing the rate capability of Si-based anodes, with major attentions paid to geometry tailoring, such as decreasing dimensions of Si particles to the nanoscale level to shorten transport pathways for both electrons and Li^+ ions [5,6], and composition modification, such as preparing various Si–C and Si–conductive polymer composites to improve surface electronic conductivity [7,8]. Even though exciting results have been achieved by such strategies, the electronic conductivity of Si itself remains low due to its intrinsic semiconductor nature, which limits the further improvement of rate capability. Carrier doping has been well established as an effective way to increase electronic conductivity of Si in the semiconductor industry [9]. However, in the field of LIBs, doping silicon with elements such as boron has been mainly employed to produce porous Si materials by wet etching [10], while the effects of doping on the rate capability of Si-based anode materials have not been intensively studied. Wang et al. reported phosphorus-doped Si film on virus enabled 3D current collectors using a physical vapor deposition technique, which exhibited improved rate performance [11]. We previously demonstrated a micro-sized Si–C composite featuring interconnected Si and carbon nanoscale building blocks that showed excellent cycling stability and rate capability [12]. The synthetic route can be easily extended to prepare doped Si-based composites by simply introducing dopant precursors during thermal disproportionation of SiO. Herein, we report a facile preparation of a boron-doped Si–C composite (B-doped Si–C) and investigate the effects of boron doping on rate capability.

2. Material and methods

The preparation procedures of boron-doped micro-sized Si–C composite are the same for our previously reported Si–C composite [12], except a mixture of SiO powder (325 mesh, Sigma Aldrich) and B_2O_3 powder (Alfa Aesar) with molar ratio of Si: B as 10:1 was used as the starting material. The products before and after carbon coating are designated B-doped Si and B-doped Si–C, respectivley. Undoped micro-sized Si–C composite is also produced for comparison and designated Si–C.

The obtained samples were characterized on a Rigaku Dmax-2000 X-ray powder diffractometer (XRD) with Cu Kα radiation. Scanning electron microscope (SEM) and transmission electron microscope (TEM) images were taken by an FEI Nova NanoSEM 630 and JEOL-1200. X-ray photoelectron spectroscopy (XPS) was conducted with a Kratos Analytical Axis Ultra XPS. Raman spectroscopy was performed with a WITec CMR200 confocal Raman instrument.

Electrochemical experiments were performed using coin cells with Li metal as the counter electrode. The working electrodes consist of 80 wt% of active material and 20 wt% of poly(acrylic acid) binder. 1 M $LiPF_6$ in a mixture of ethylene carbonate, diethyl carbonate and dimethyl carbonate (2:1:2 by volume) and 10 wt% fluoroethylene carbonate

* Corresponding author. Tel.: +1 814 863 1287.
E-mail address: dwang@psu.edu (D. Wang).

1388-2481/$ – see front matter © 2013 Elsevier B.V. All rights reserved.
http://dx.doi.org/10.1016/j.elecom.2013.09.004

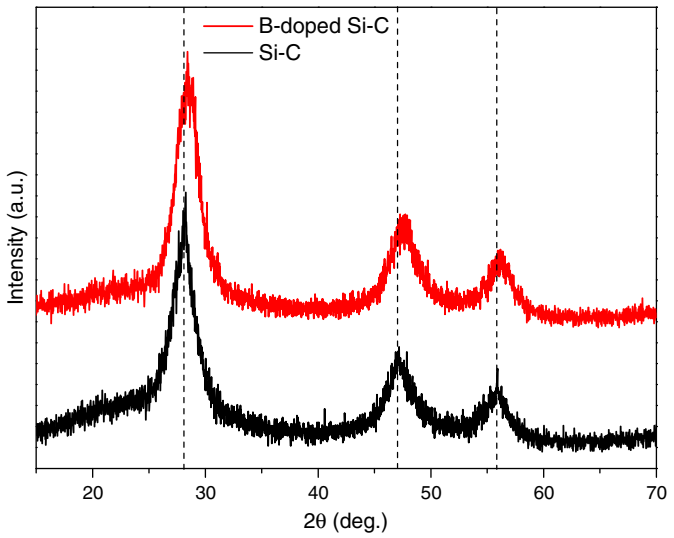

Fig. 1. XRD patterns of Si–C and B-doped Si–C.

was used as electrolyte. The mass loading of active materials is 1.2 mg/cm^2. Galvanostatic charge/discharge tests were carried out on an Arbin BT-2000 battery tester between 1.5 and 0.01 V versus Li^+/Li. Electrochemical impedance spectroscopy (EIS) was carried out by applying a perturbation voltage of 5 mV between 10 mHz and 100 KHz using a Solartron SI 1260 impedance analyzer. Powder conductivity was measured using a Solartron SI 1287 electrochemical interface.

3. Results and discussion

The phase and crystallinity of Si–C and B-doped Si–C were examined by XRD. Peaks of both XRD patterns can be indexed to those of face-centered cubic crystalline Si (JCPDS Card No. 27-1402), as shown in Fig. 1. Compared to undoped Si–C, the peaks of B-doped Si–C shift to higher angles due to the replacment of Si atoms by smaller B atoms which leads to a smaller lattice constant [13]. This result, combined with the absence of Si–B alloy peaks, indicates the successful doping of B into Si. No discernable difference in peak intensities can be found, suggesting that B doping did not affect crystallinity of the final product. The nature of Si and B in B-doped Si before carbon coating was

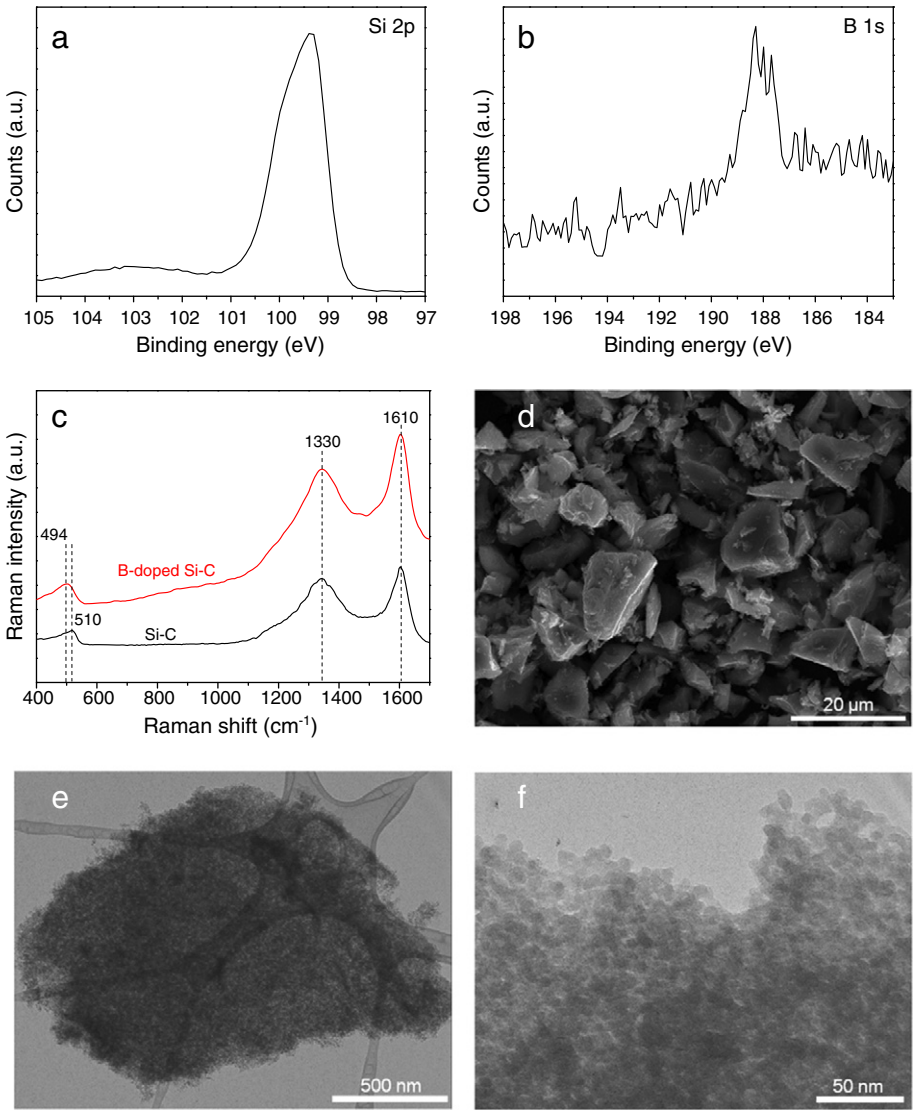

Fig. 2. (a) Si 2p and (b) B 1s XPS spectra, and (c) Raman spectra of B-doped Si–C and Si–C, (d) SEM image, (e) low- and (f) high-magnification TEM images of B-doped Si–C.

investigated by XPS. As shown in the Si 2p spectrum in Fig. 2a, the strong peak at 99.4 eV corresponds to the binding energy of Si(0) [14]. A broad weak bump is also observed around 103 eV, which suggests the existence of silicon oxides [15]. Fig. 2b shows the B 1s spectrum, which is rough due to the very low relative sensitivity of boron [16]. The peak centered at 188 eV is attributed to B(0) [16], serving as direct evidence of B doping. The content of B is calculated to be 4.1% (atomic percentage) by XPS survey, close to the designated composition of 5%. Raman spectroscopy was employed to further study the B-doped Si after carbon coating. The Si peak shifts from 510 cm^{-1} for undoped Si to 494 cm^{-1} for B-doped Si (Fig. 2c) due to disorder in the Si structure caused by the stress developed in the surrounding Si atomic network after B doping, which is consistent with the previous report [17] as well as with XRD and XPS results above. It has been reported that B doping into carbon can enhance electrochemical performance of resultant B-doped carbon [18,19]. However, in our case B in carbon was not detected as shifting of C peaks is not observed [18]. As shown in Fig. 2c, both spectra show peaks around 1330 and 1610 cm^{-1}, corresponding to the D and G bands of carbon, respectively [12]. The absence of B in carbon is due to the moderate carbon coating temperature of 620 °C, much lower than the temperature (900–2800 °C) required for B doping in carbon *via* solid state diffusion [19,20].

The morphology, size, and structure of the B-doped Si–C composite were also investigated by SEM and TEM. The SEM image in Fig. 2d shows that the B-doped Si–C is composed of micro-sized particles with an average size of about 20 μm. TEM study reveals that these micro-sized particles are built up of interconnected nanoparticles with a size of about 10 nm (Fig. 2e and f). This shows that B doping has no influence on the size and structure of product, as the same features are observed for the undoped Si–C composite [12].

The doping effects on the electrochemical performance was evaluated by galvanostatic charge/discharge at different current densities. To examine the effects of B doping only, potential interference factors were excluded. First, electrodes were prepared without any external carbon additive. Second, to exclude the influence of carbon content, a similar carbon content of around 20 wt% (measured by elemental analysis) was achieved for both B-doped Si–C and Si–C.

As shown in Fig. 3a, B-doped Si–C exhibits similar specific capacity to Si–C at 400 mA/g due to the low content of B as discussed above. However, the difference in capacity can easily be observed at higher current densities. For example, Si–C can only achieve 323 mAh/g cycling at 6.4 A/g. In comparison, a capacity of 575 mAh/g (volumetric capacity of 449 mAh/cm^3 based on tap density of 0.78 g/cm^3) can be obtained for B-doped Si–C, about 80% higher than that of Si–C and 1.5 times the theoretical capacity of graphite. Note that this capacity was achieved without addition of any external conductive additive, which is usually present in large quantity (more than 20 wt%) in reports on Si-based materials with good high rate performance [10]. After the current density was restored to 400 mA/g, B-doped Si–C showed better stability than Si–C with similar capacity. The coulombic efficiency (CE) of B-doped Si–C remains above 99.5% at various rates. To further investigate the cycling stability at high rates, the current density was increased from 400 mA/g to 6.4 A/g again. In contrast to the obvious capacity fading of Si–C, the capacity of B-doped Si–C was stable for about 50 cycles at 6.4 A/g. Fig. 3b plots the ratio of specific capacities of B-doped Si–C and Si–C at different current densities. It is clear that the difference in specific capacities becomes more and more striking with increasing current density. The voltage profiles of B-doped Si–C at various current densities are shown in Fig. 3c. The first cycle CE is 73.7%, similar to that of Si–C (Fig. 3a). The kinetic feature of charge/discharge curves is maintained at high rates, as the voltage profiles remain similar in shape with increasing current density, indicating a facile charge transport process. To understand the reason for the better rate capability of B-doped Si–C, cells were analyzed by the EIS measurements after rate capability testing at delithiated state. The inclined line in the low frequency region is related to Li-ion diffusion within particles [21]. The difference is indicative of change in Li-ion diffusion behaviors due to boron doping, which agrees well with the report that addition of dopants such as boron and phosphorus to Si strongly influences the energetics and kinetics of Li insertion [22]. B-doped Si–C

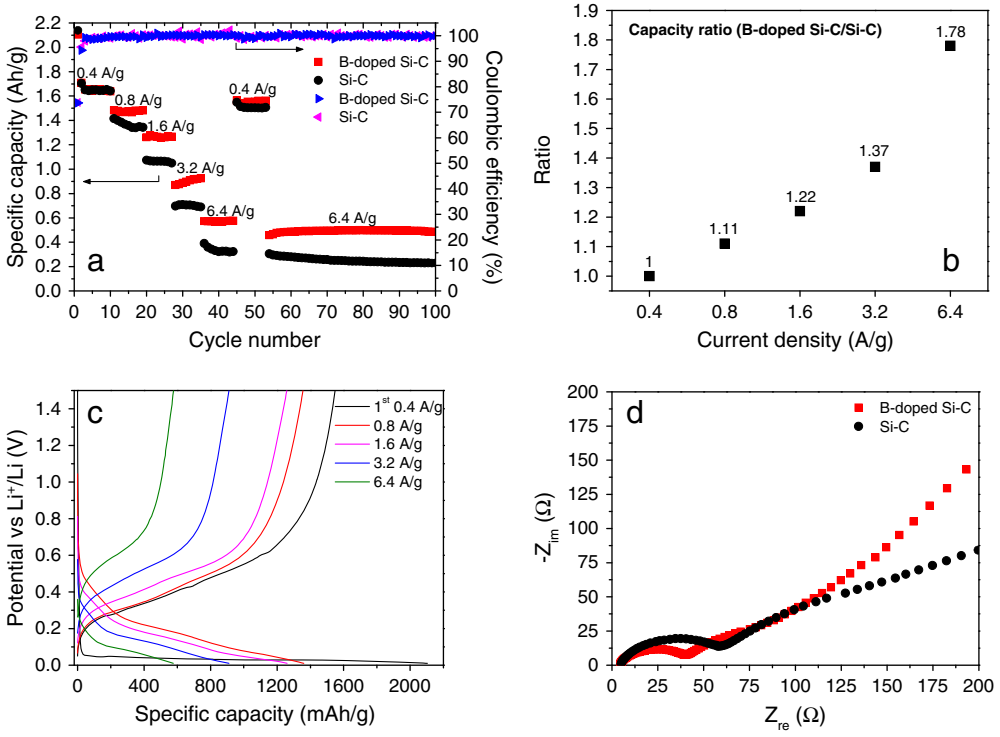

Fig. 3. (a) Rate performance and (b) capacity ratio at different current densities of B-doped Si–C and Si–C. (c) Voltage profiles at different current densities of B-doped Si–C. (d) Impedance spectra of B-doped Si–C and Si–C.

shows a smaller semicircle in high-to-medium frequency region than Si–C, which suggests a lower charge transfer resistance [21]. The electronic conductivities of B-doped Si–C and Si–C powder were also measured according to a reported protocol [23]. Compared to 9.6×10^{-6} S/m of Si–C, B-doped Si–C has higher conductivity of 3.6×10^{-4} S/m. The results indicate that boron doping leads to an increase in electronic conductivity of the Si–C composite and thus improves its rate capability.

4. Conclusions

In summary, a boron-doped Si–C composite has been successfully prepared and the boron doping was confirmed by XRD, XPS, and Raman spectrometry. The effects of boron doping on the rate capability of the Si–C composite have been investigated. Compared to undoped Si–C, the B-doped Si–C composite exhibits much improved rate capability. A high capacity of 575 mAh/g can be achieved by B-doped Si–C at 6.4 A/g, about 80% higher than that of Si–C. The improved rate capability is attributed to lower charge transfer resistance of B-doped Si–C, as shown by EIS measurement. The finding demonstrates that boron doping is an effective approach to enhance rate capability of Si-based anodes for LIBs.

Acknowledgments

This work was supported by the Assistant Secretary for Energy Efficiency and Renewable Energy, Office of Vehicle Technologies of the U.S. Department of Energy under Contract No. DE-AC02-05CH11231, Subcontract NO. 6951378 under the Batteries for Advanced Transportation Technologies (BATT) Program.

References

[1] M.S. Whittingham, Chem. Rev. 104 (2004) 4271.
[2] S. Hossain, Y.-K. Kim, Y. Saleh, R. Loutfy, J. Power Sources 114 (2003) 264.
[3] B.A. Boukamp, G.C. Lesh, R.A. Huggins, J. Electrochem. Soc. 128 (1981) 725.
[4] T. Song, H. Cheng, H. Choi, J.-H. Lee, H. Han, D.H. Lee, D.S. Yoo, M.-S. Kwon, J.-M. Choi, S.G. Doo, H. Chang, J. Xiao, Y. Huang, W.I. Park, Y.-C. Chung, H. Kim, J.A. Rogers, U. Paik, ACS Nano 6 (2011) 303.
[5] M.-H. Park, M.G. Kim, J. Joo, K. Kim, J. Kim, S. Ahn, Y. Cui, J. Cho, Nano Lett. 9 (2009) 3844.
[6] Z. Wen, G. Lu, S. Mao, H. Kim, S. Cui, K. Yu, X. Huang, P.T. Hurley, O. Mao, J. Chen, Electrochem. Commun. 29 (2013) 67.
[7] S. Chen, M.L. Gordin, R. Yi, G. Howlett, H. Sohn, D. Wang, Phys. Chem. Chem. Phys. 14 (2012) 12741.
[8] H. Wu, G. Yu, L. Pan, N. Liu, M.T. McDowell, Z. Bao, Y. Cui, Nat. Commun. 4 (2013).
[9] A.V. Krasheninnikov, K. Nordlund, J. Appl. Phys. 107 (2010) 071301.
[10] M. Ge, J. Rong, X. Fang, C. Zhou, Nano Lett. 12 (2012) 2318.
[11] X. Chen, K. Gerasopoulos, J. Guo, A. Brown, R. Ghodssi, J.N. Culver, C. Wang, Electrochim. Acta 56 (2011) 5210.
[12] R. Yi, F. Dai, M.L. Gordin, S. Chen, D. Wang, Adv. Energy Mater. 3 (2013) 295.
[13] J.M. Baribeau, S.J. Rolfe, Appl. Phys. Lett. 58 (1991) 2129.
[14] N. Liu, H. Wu, M.T. McDowell, Y. Yao, C. Wang, Y. Cui, Nano Lett. 12 (2012) 3315.
[15] R. Yi, F. Dai, M.L. Gordin, H. Sohn, D. Wang, Adv. Energy Mater. (2013), http://dx.doi.org/10.1002/aenm.201300496.
[16] X.J. Hao, E.C. Cho, C. Flynn, Y.S. Shen, G. Conibeer, M.A. Green, Nanotechnology 19 (2008) 424019.
[17] S.R. Jadkar, J.V. Sali, M.G. Takwale, D.V. Musale, S.T. Kshirsagar, Sol. Energy Mater. Sol. Cells 64 (2000) 333.
[18] I. Mukhopadhyay, N. Hoshino, S. Kawasaki, F. Okino, W.K. Hsu, H. Touhara, J. Electrochem. Soc. 149 (2002) A39.
[19] Y. Jae-Seong, J. Sang-Min, M. Jin, A. Bai, M. Isao, R. Choong Kyun, Y. Seong-Ho, Nanotechnology 23 (2012) 315602.
[20] W. Han, Y. Bando, K. Kurashima, T. Sato, Chem. Phys. Lett. 299 (1999) 368.
[21] E. Pollak, G. Salitra, V. Baranchugov, D. Aurbach, J. Phys. Chem. C 111 (2007) 11437.
[22] B.R. Long, M.K.Y. Chan, J.P. Greeley, A.A. Gewirth, J. Phys. Chem. C 115 (2011) 18916.
[23] A. Celzard, J.F. Marêché, F. Payot, G. Furdin, Carbon 40 (2002) 2801.